ELSEVIER

Tectonophysics 283 (1997) 129–143

TECTONOPHYSICS

Heterogeneous strain associated with normal faulting: evidence of mass transfer by pressure solution associated with fault displacement

Pascale Canole, Francis Odonne *, Mireille Polve

CNRS UMR n°5563, Institut des Sciences de la Terre, Université Paul Sabatier 38, rue des Trente-six-Ponts, F-31400 Toulouse, France

Received 18 June 1996; accepted 9 April 1997

Abstract

In a well stratified flysch in the French Pyrenees, the offset of layers along a fault zone provide good data of relative displacement. It is shown that the fault surface is composed of three right-stepping fractures that opened tensile bridges along small left-stepping fractures. Translation on the fault zone is parallel to the fault surface. The displacement vector field shows that the movement between the two blocks was not a rigid body translation and that deformation in the hanging wall is greater than that in the foot wall. Volume loss within the rock is compensated by volume increase close to the fault surface.

Calcite dissolution and reprecipitation by pressure solution is indicated by the occurrence of stylolites and numerous calcite-filled veins around the fault. Calcite dissolution is more important in the hanging wall, especially in layers where the calcite content is close to 60%. Both cathodoluminescence observations and rare-earths element patterns are in favour of calcite in veins and dominos coming from units adjacent to the fault. There is no evidence that some calcite coming from farther distance could have entered in the system.

Keywords: strain; normal faulting; mass transfer; pressure solution

1. Introduction

A fault surface is a kinematic discontinuity along which two blocks move in opposite directions. Because faults have finite dimensions, the displacement does not have a constant value along the fault surface (Walsh and Watterson, 1989) and must be accommodated by strain. This strain is concentrated at fault tips (Chinnery, 1961; Rispoli, 1981; Pollard and Segall, 1987; Bürgman and Pollard, 1994) but it is not strictly limited to these areas. The rotation of a fault (Freund, 1970) and the bending of its surface (Freund, 1974; Gapais et al., 1991) are good evidences for a wider distribution of strain.

Large amounts of strain generally require ductile processes. In many cases, pressure solution has been recognized as the mechanism which can account for a large part of strain around faults (Carrio-Schaffhauser and Chenevas-Paule, 1989; Carrio-Schaffhauser and Gaviglio, 1990; Odonne, 1990; Gratier and Gamond, 1990; Peacock and Sanderson, 1995). One of the principal parameters to be assessed concerns the size of the system involved in such a process. This requires a knowledge of the displacement along the fault and of the amount of mass transfer around the fault. Ge-

* Corresponding author. Fax: +33-05-61 52 05 44. E-mail: odonne@cict.fr

PII S0040-1951(97)00074-7

ometrical data can provide direct information on the displacement. From the analysis of the vector field, it is possible to reconstruct the strain undergone by the matrix (Ramsay and Huber, 1983) and to identify the domains where volume, or area, has changed. When distinct layers are present in the rock, their relative offset provides good measurements of displacement along the fault surface. The aim of this study is to provide such geometrical data and chemical data collected on a selected fault.

We have selected an outcrop of flyschs from the French Western Pyrenees where the occurrence of numerous veins and stylolites clearly shows the importance of pressure solution during deformation. As a complement to geometrical data and in order to determine the size of the system involved in mass transfer, some major elements (Ca, Fe etc.) and rare-earths elements have been measured to characterize the geochemical signature of each layer, its variation in relation with the fault plane, and to try to identify the origin of the calcite that has migrated into the system.

2. Kinematic analysis

2.1. *The shape of the fault surface*

Cretaceous flyschs are common geological units in the Western French Pyrenees. Near Saint-Jean-de-Luz (along the Atlantic coast, Pays Basque), the shore cliffs provide numerous and well exposed outcrops of these well stratified sedimentary rocks. All are mixtures of detrital and carbonaceous components. On the outcrop soft marly layers alternate with more competent carbonaceous-rich layers. Locally, normal faults can be observed, cutting across the horizontal layers. We have selected the fault presented in the Fig. 1 for measuring the displacement because of its small scale, excellent exposure, and its isolated situation, relative to other faults. The fault is

Fig. 1. View of the fault zone in the Cretaceous flysch near Saint-Jean-de-Luz (French Pyrenees). The fault is composed of small left-stepping fractures opened during the displacement along three longer right-stepping fractures. Fibres on the fault surface indicate a normal dip-slip displacement.

a few metres long and its two tips are clearly exposed in the outcrop. Fibres on the fault surface indicate a perfect dip-slip displacement lying within the plane of Fig. 1. There is not any indication of oblique displacement on this fault or on the adjoining ones. This fault is a part of a larger folded structure in which a single stage of deformation has been described (Robert, 1979). For each layer displaced along the fault surface, the length of the fibres equals the offset of the layer. All this suggests that the calcite fibres represent a complete picture of displacement on the fault surface.

The fault surface is composed of three right-stepping shear fractures that are connected by short left-stepping fractures. The overall displacement on the fault zone has caused the long fracture segments to slip and the short fracture segments to open. The angle between the two sets of fractures is greater than 45° everywhere on the fault, reaching 48° and 52° in the middle and lower parts of the fault, respectively (Fig. 2). The angle in the calcite domino above the fault although not clear, appears to be more than 50°. Such angular relationships between the two sets of fractures are interpreted as being the result of tensile bridges opening along the first generation of right-stepping fractures (Gamond, 1987).

It is possible to determine the infinitesimal direction of displacement from these two sets of fractures (Mc Coss, 1986; Peacock and Sanderson, 1995). In the three points where a simple geometrical construction has been possible (Fig. 2b), the displacement vectors show a displacement parallel to the fault surface. In fact, a minor transtensional component can also be observed.

2.2. Displacement vector field

On the fault surface, the relative displacement of the layers, the opening of the calcite dominos, and the elongation of the fibres, all provide good indications of the direction of displacement. The initial shape of the fault and its vicinity can be restored by undoing the offset of each layer. In order to perform this reconstruction, a grid is drawn as an overlay on the line drawing of the fault (Fig. 3a). This overlay is then cut and each block is displaced to restore the unbroken shape of each layer before fracturing. To obtain the best fit, some of the blocks need to be divided in sub-blocks (Fig. 3b). The relative displacement vectors (Ramsay and Huber, 1983) were drawn by joining the initial (Fig. 3b) and the final (Fig. 3a) positions of the grid intersections. The vectors show the normal dip-slip displacement of the upper block and anticlockwise rotation of the blocks and the fault trace (Fig. 4). Similar block and fault rotations have been described in other natural examples (Frei and Freund, 1990; Odonne and Massonnat, 1992) and in analogue experiments (Gapais et al., 1991; Schreurs, 1994). The displacement vector field clearly shows that the displacement along the fault trace does not indicate a rigid body translation of the blocks and rather, represents a heterogeneous strain (Ramsay and Huber, 1983).

2.3. Strain analysis

The finite strain is estimated by superimposing the small squares of the grid onto the corresponding parallelogram reconstructed from the undeformed shape (Fig. 5). This superimposition shows the local displacement vectors and the related strain for each square. The hanging wall appears to have been much more deformed than the foot wall (Fig. 5).

The change in area which has accompanied the deformation is measured by comparing the area of each small square to the one of the corresponding parallelogram at the undeformed stage (Fig. 5). Most of the changes in area that are recorded around the fault are negative and are mainly located in the hanging wall of the fault (Fig. 6). The largest changes in area are located in the lower half of the hanging wall while, in the foot wall, the only change is located close to the top of the block (Fig. 5). These symmetrical points of highest negative area change correspond to the domains which have undergone compression around the fault tips (Chinnery, 1961; Rispoli, 1981).

Positive area changes are scarce but have higher values. These positive area changes are located exactly on the fault plane in the calcite dominos (Fig. 6).

In order to evaluate how volume losses and gains are balanced, the area of the central part of the fault (Fig. 3a) was compared with the corresponding part in the reconstructed space (Fig. 3b). The area of the deformed part, given in arbitrary values, is A def. $= 96.39$ for the area of the deformed part, and the

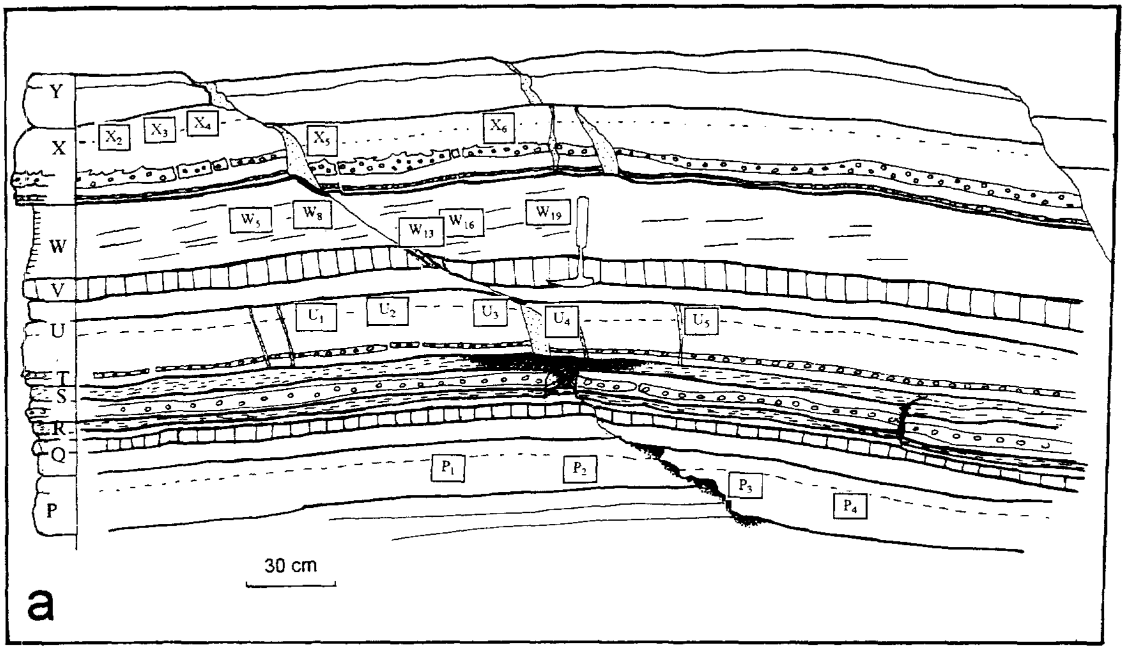

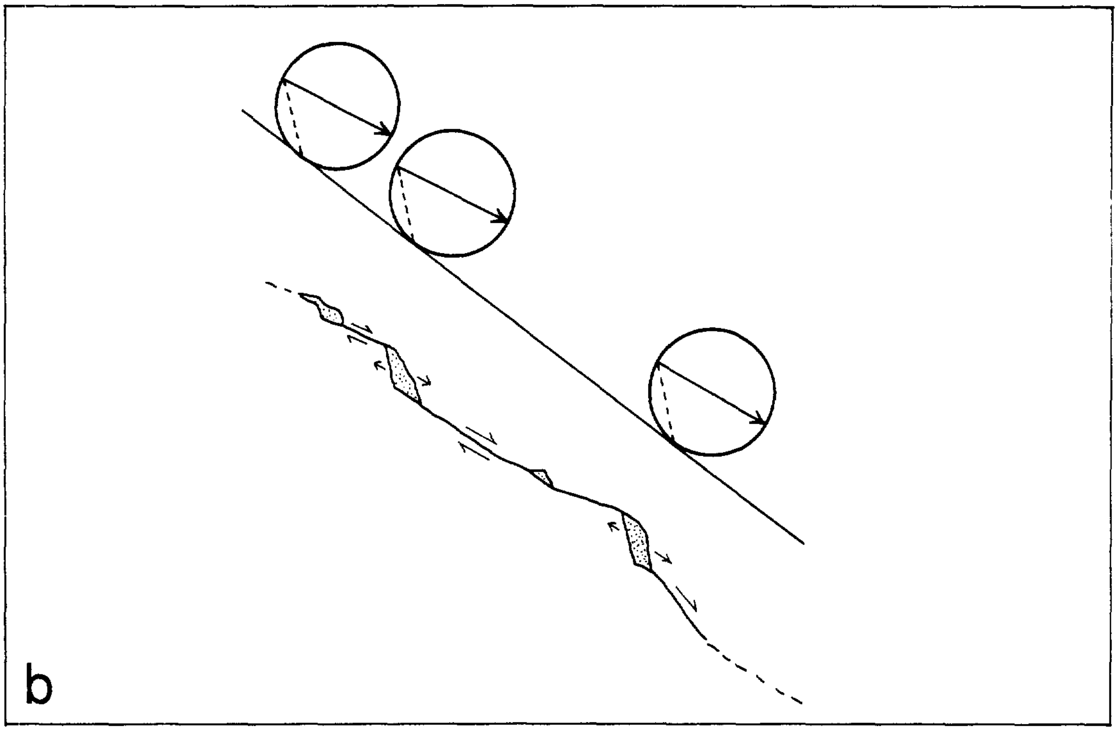

Fig. 2. (a) Line drawing of the fault and layers in Fig. 1. Location of samples analysed for REE is given. (b) Angular relationship between the two sets of fractures. The arrows inside the circles give the infinitesimal displacement direction (Peacock and Sanderson, 1995) that has been determined in three points along the fault zone. The displacement on the fault surface is almost parallel to the fault direction.

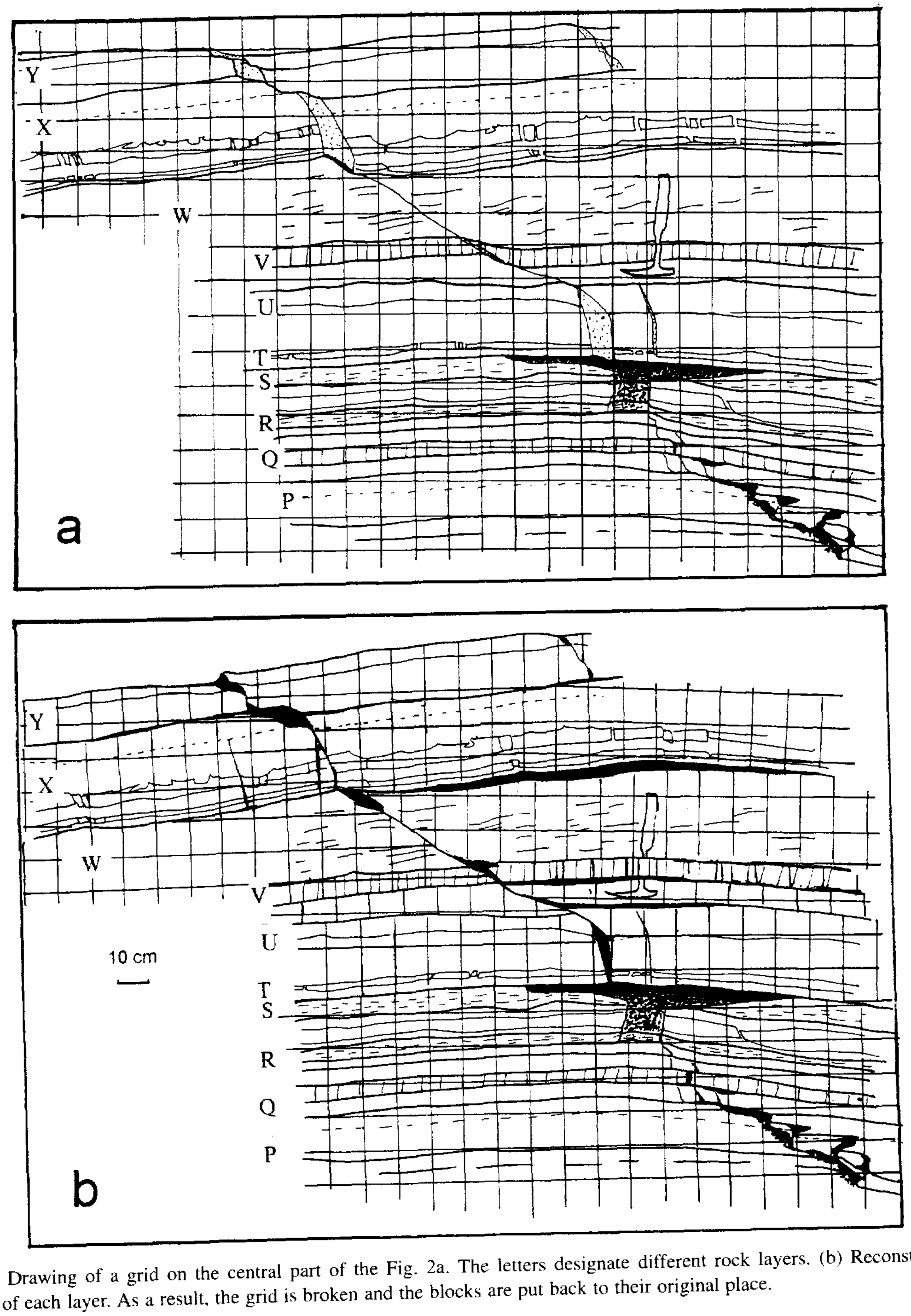

Fig. 3. (a) Drawing of a grid on the central part of the Fig. 2a. The letters designate different rock layers. (b) Reconstruction of the continuity of each layer. As a result, the grid is broken and the blocks are put back to their original place.

corresponding reconstructed area, A rec. = 97.09. The ratio between deformed and reconstructed areas is roughly 1 (A def./A rec. = 0.9928) showing that negative and positive area changes are well balanced and that the overall volume was conserved during the deformation.

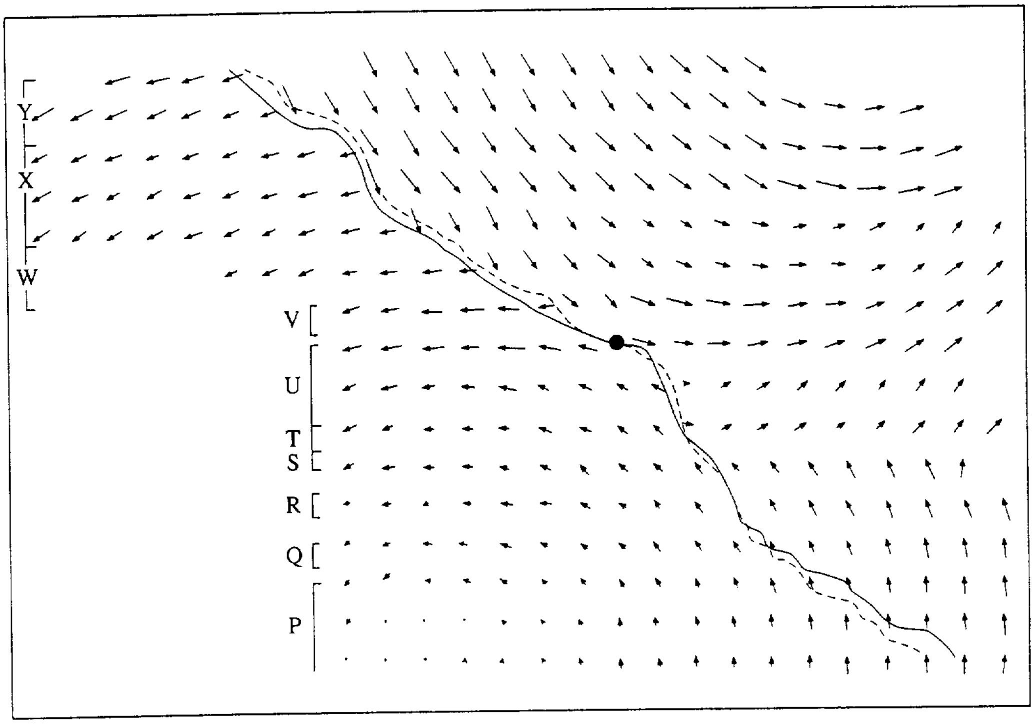

Fig. 4. Relative displacement vector field drawn by joining the initial positions (Fig. 3b) and the final positions (Fig. 3a) of the grid nodes. The blocks and the fault zone have non rigidly translated and rotated in an anticlockwise direction in a heterogeneous strain field. The black point indicate the origin of the reference frame.

3. Deformation mechanism, pressure solution

In order to find out whether changes in area, or in volume, during deformation are the result of compaction, porosity measurements by helium expansion were carried out on eighteen samples from the S, U and X layers (Fig. 1) taken from a distance of a few metres from the fault. In none of the samples, porosity exceeds 2%. Such low values exclude porosity as a major factor in local volume changes that can reach 20% (Fig. 6). A process other than compaction must be responsible for volume changes in this outcrop.

Calcite dominos along the fault surface and numerous veins associated with stylolites, in the matrix, indicate the occurrence of pressure solution (Fletcher and Pollard, 1981). Stylolite which is particularly developed in $CaCO_3$-rich layers was studied in thin section. Fig. 7 is a line drawing of a thin section depicting a stylolite (horizontal feature) and two veins (vertical features) that are filled with calcite. The small vein on the left hand side of the figure is filled with fibres, while the larger vein, on the right, is filled with equidimensional crystals. The fibres indicate a very slow, aseismic displacement (Ramsay, 1980), while large equidimensional crystals fill a cavity that probably opened by high rate displacement (Gratier and Gamond, 1990) during a seismic event. In the centre of Fig. 7, the horizontal stylolite dissolved some of the fibres in the small vein and in turn is cut and moved apart by the larger vein. This observation implies that the stylolite formed after the small vein but before the large one. Analysis of 24 thin sections show stylolites cutting and being cut by veins, indicating their coeval formation.

4. Estimation of mass transfer

4.1. Evaluation of the volume that underwent pressure solution

Pressure solution is probably the mechanism responsible for the mass transfer observed around the

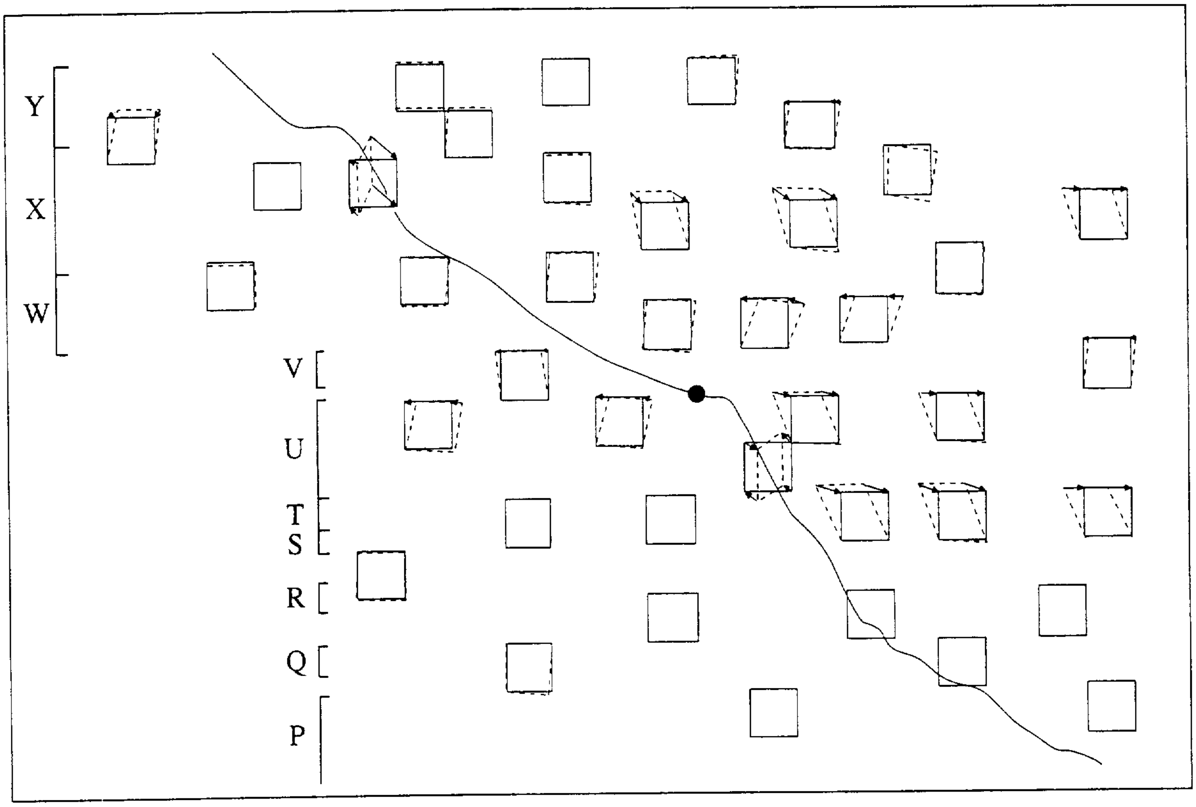

Fig. 5. Superimposition of some of the squares from the grid of Fig. 3a and their reconstructed shapes in Fig. 3b. The local displacement vectors show that the strain is concentrated in the hanging wall.

fault. If so, since calcite dissolves in the stylolites and crystallizes in veins, it should be possible to detect changes in the calcite contents of the layers. However, we must first verify that calcite was initially homogeneously distributed in each layer. One way to do this is to check the variability of immobile elements ratios (Gratier, 1983) along each layer, far from the fault. Homogeneous layers must have constant ratios between all elements before deformation. After deformation, the ratios of soluble elements may have changed but the ratio of each immobile element to the total amount of immobile elements should be the same. Concentrations of Al_2O_3, Fe_2O_3, TiO_2 and K_2O were measured in the P, U, X and W layers (Fig. 8 and Table 1). For each layer, four or five samples were measured across the fault. For each sample, element concentrations are normalized to the sum of immobile elements (Fig. 8). Each layer has a specific ratio of insoluble elements and, except for P_3 and X_6, this ratio is fairly constant within the layer. The change in X_6 seems to be independent compared to the position of the fault (dashed line in the figure), this is less clear in the case of P_3. The reasonably constant ratios of insoluble elements shows that the layers had a roughly homogeneous composition before deformation. Then lateral change in calcite content can be attributed to mass-transfer processes occurring during deformation.

Calcite contents were measured by calcimetry in more than 80 locations in the outcrop. The precision of these measurements have been checked by duplicating twenty analyses by ICP–AES; the difference between the two results is always below 1 %.

Calcite analyses show an almost systematic difference between the two blocks of the fault, as shown in Fig. 9. For each layer, the calcite content is generally lower in the hanging wall of the fault. In some places, the difference can reach 10%. Calcite deple-

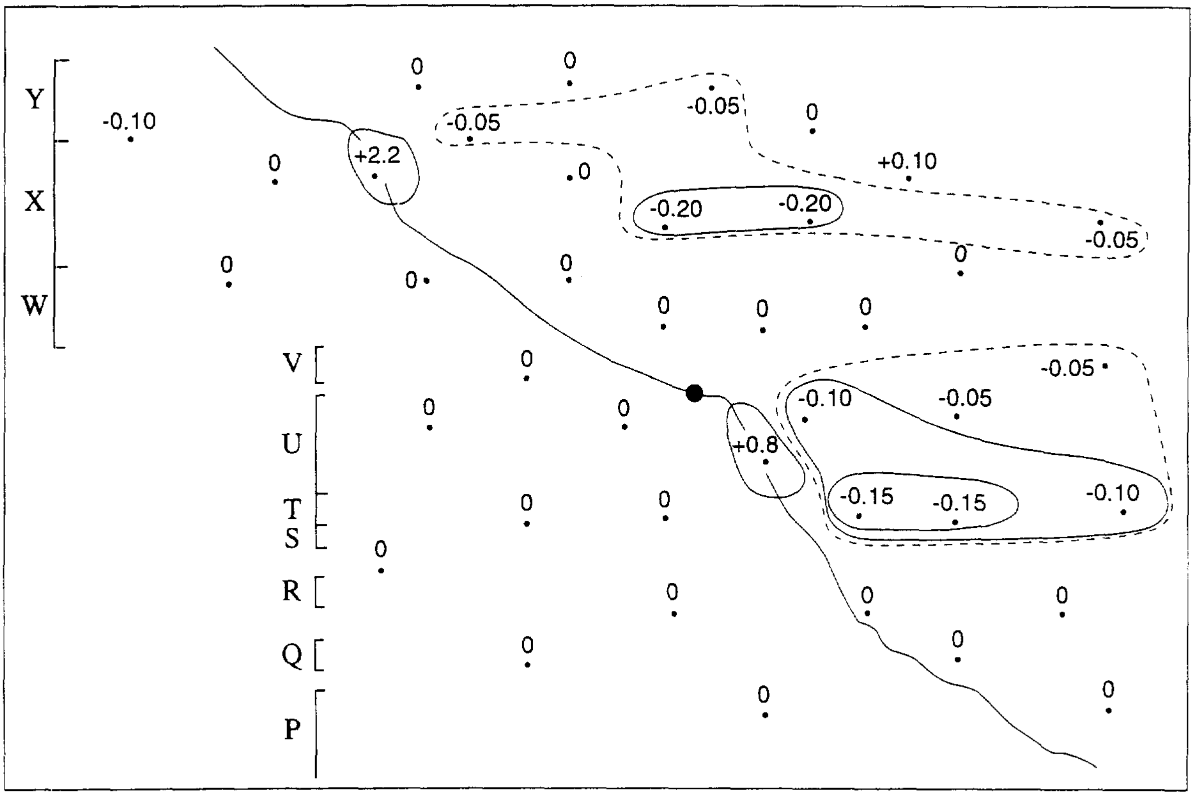

Fig. 6. Spatial variation of the change in area determined by comparing the area of each small square to that of the corresponding parallelogram. Positive area changes are located on the fault surface or close to it. Most of the area changes are negative and are distributed in the upper block.

tion extends to about one metre away from the fault. On the left side of the fault (foot wall) this depletion is smaller and appears to be limited to within a few decimetres of the fault surface. This suggests that the amount of mass transfer is different in the two blocks.

The amount of mass transfer also appears to be different within each layer, in relation with its chemistry. This amount of mass transfer can be expressed as $\Delta V/V$ (amount of volume change). When the system is closed, Gratier (1983) has shown that:

$$\Delta V/V = (I_p - I_e)/(I_p + I_e)$$

where I_p and I_e are the concentration of insoluble elements (Al_2O_3, Fe_2O_3, K_2O and TiO_2) in the protected area and in the area exposed to deformation, respectively. Here, because the overall volume was conserved during the deformation (see Fig. 3 and comments), the system is thought to be closed. We applied the above-mentioned formula using either complete chemical analyses or data from calcimetry. In this latter case, because $CaCO_3$ appears to be the only mobile part, insoluble elements are considered to be all that is not $CaCO_3$. These measurements of $\Delta V/V$ are compared to the amount of area changes that have been reconstructed in Fig. 6.

Chemical analyses exist from four layers: P, U, W and X, calcimetry measurements come from all layers and measurements of area changes come from all layers, except P. The different measurements give three curves of $\Delta V/V$ versus the different layers. They are plotted in Fig. 10. The curves show a good agreement between the different methods. They all show maximum and minimum values in the same layers. Then, using the data from calcimetry, the area of volume loss — $\Delta V/V$ (Gratier, 1983) — can be located around the fault in the hanging wall

Fig. 7. Line drawing of two veins filled with calcite (vertical in the picture). On the left, the vein is filled with fibres and the vein on the right is filled with equidimensional crystals. In the middle of the figure, an horizontal stylolite intersects the small fibrous vein while it is cut by the larger vein on the right. These textures indicate that the stylolite formed after the small vein but before the larger vein.

(Fig. 11). The volume loss is large — 24.7% — in layers where $CaCO_3$ content is about 90% because a large solution of $CaCO_3$ is possible and give a large volume loss. At the opposite the volume loss is very low — from 0.7 to 3.1% — when the $CaCO_3$ content is minus than 60%. The volume loss is moderate — about 10% — when the $CaCO_3$ content is between 60 and 80%.

This can be related to the mechanism of pressure-solution. Layers with high calcite content can undergo large dissolution and are expected to show large values of volume loss. In the same time, the high insoluble contents help the dissolution process, either by increasing the kinetics of the reaction or by producing some high speed paths for mass transfer (Heald, 1956; Weyl, 1959; Gratier, 1987). It also appears that soluble components are not easy to remove from layers with high contents in clay minerals. This is probably why the largest values of volume loss are observed in layers where calcite contents is large, more than 60%. In layers where $CaCO_3$ content is minus than 60%, solution is very moderate and volume loss too.

4.2. *Origin of the calcite*

The analysis of major elements and stylolite show that local mass transfer involved principally $CaCO_3$, from the deformed areas to the fault surface or its surroundings. The calcite could have a dual origin: partly transferred from the surrounding rocks and partly introduced into the system via fluids. To investigate this question we have chosen two techniques: (1) observation of thin sections under cathodoluminescence and (2) analysis of rare-earth elements by ICP/MS.

Cathodoluminescence is helpful in recognizing zoning in crystals or cements as it produces various colour zones with different activated trace elements. Observations of all of our thin sections with cathodoluminescence show that all the calcite crystals observed in the veins, on the fault surface and in the

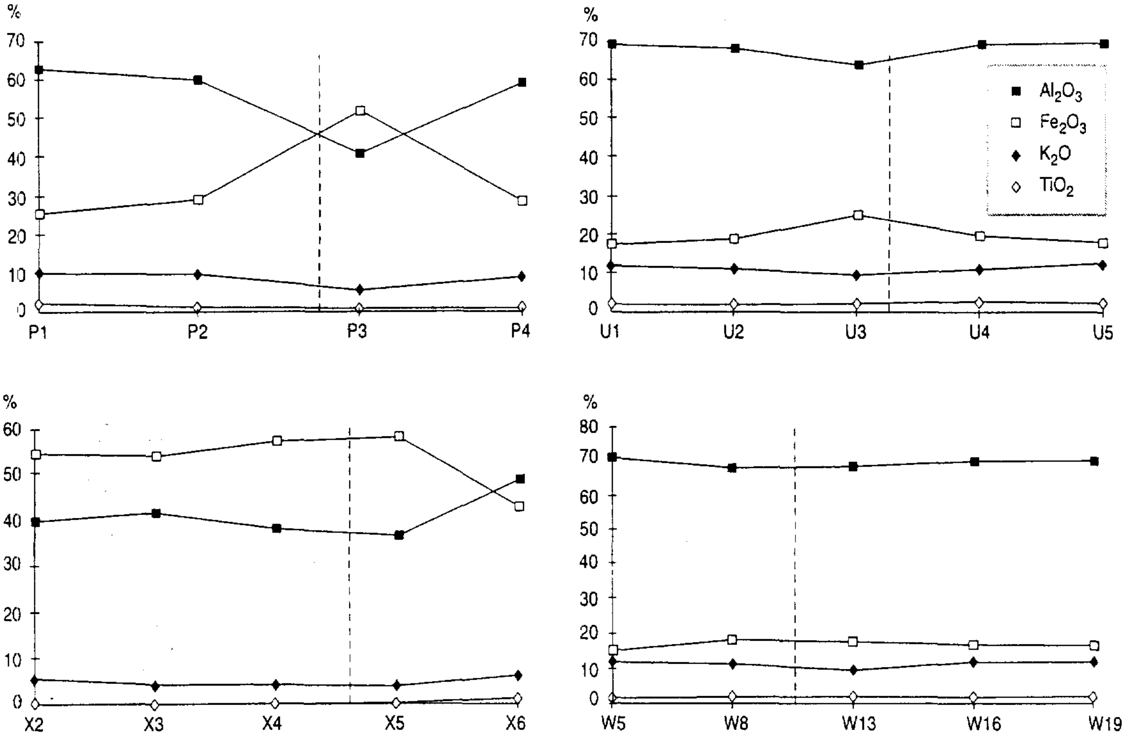

Fig. 8. The distribution of Al_2O_3, Fe_2O_3, K_2O and TiO_2 normalized to the sum of immobile components measured in the layers P, U, X and W (cf. Fig. 2). In each layer, four or five samples have been measured across the fault. Each layer has a specific ratio of insoluble elements which except for P_3 and X6, remains generally constant in all layers. The changes seem to be independent of the distance from the fault which is indicated by the vertical dashed line.

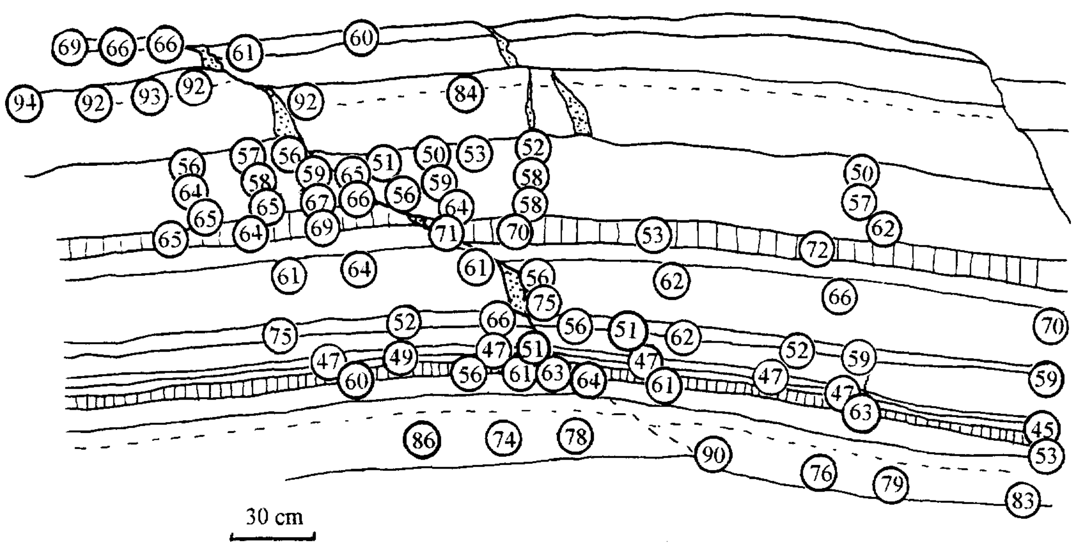

Fig. 9. The distribution of the calcite content on the outcrop is given in percent. The upper block appears to be depleted in calcite over a distance of one metre in some layers.

Table 1
Major element analyses measured in the P, U, X and W layers

Samples	SiO_2	Al_2O_3	Fe_2O_3	MnO	MgO	CaO	Na_2O	K_2O	TiO_2	P_2O_5	LOI
P1	17.91	2.9	1.17	0.04	0.7	41.51	0.21	0.48	0.08	0.07	34.71
P2	14.75	2.43	1.17	0.04	0.62	43.96	0.17	0.39	0.06	0.07	36.12
P3	5.86	0.79	1	0.04	0.39	50.24	0.05	0.11	0.02	0.05	40.61
P4	15.79	2.56	1.23	0.05	0.67	42.52	0.16	0.41	0.08	0.06	36.24
U1	30.91	4.03	0.99	0.02	0.78	33.3	0.28	0.7	0.13	0.05	28.63
U2	31.02	3.3	0.91	0.02	0.68	33.54	0.25	0.55	0.1	0.05	29.37
U3	33.69	2.33	0.9	0.02	0.54	33.26	0.21	0.35	0.07	0.05	28.37
U4	39.63	3.2	0.88	0.02	0.63	28.99	0.26	0.49	0.1	0.05	25.57
U5	30.97	4.44	1.11	0.02	0.85	32.31	0.31	0.76	0.14	0.06	28.83
X2	3.51	0.49	0.67	0.04	0.38	52.45	0.05	0.07	–	0.05	42.06
X3	2.44	0.39	0.51	0.03	0.36	53.35	0.04	0.04	–	0.04	42.56
X4	3.21	0.42	0.63	0.03	0.34	52.53	0.04	0.05	–	0.05	41.86
X5	4.25	0.49	0.78	0.05	0.34	51.93	0.05	0.06	–	0.05	41.77
X6	10.58	1.26	1.11	0.04	0.49	47.5	0.09	0.17	0.03	0.04	38.45
W5	25.87	6.46	1.4	0.02	0.54	32.69	0.23	1.1	0.12		30.07
W8	25.57	6.42	1.74	0.02	0.95	33.2	0.35	1.08	0.19	0.06	30.19
W13	25.75	6.56	1.79	0.02	0.97	32.94	0.34	1.1	0.2	0.06	30.04
W16	26.3	6.51	1.57	0.03	0.8	32.76	0.31	1.11	0.17	0.04	29.85
W19	26.76	6.65	1.58	0.03	0.8	32.51	0.33	1.13	0.17	0.04	29.69

Measurements made at 'Centre de Recherches Pétrographiques et Géochimiques' in Nancy, France, using an Inductively Coupled Plasma Adsorption and Emission Spectrometer (ICP/AES). The high value of LOI in each sample is explained by the large amount of CO_2 coming from $CaCO_3$ decomposition.

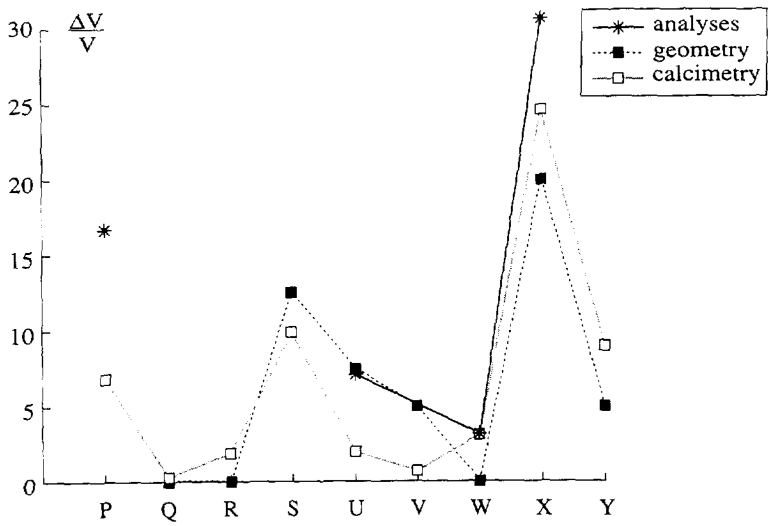

Fig. 10. Measurements of $\Delta V/V$ by using three different techniques. The first one is the result of area changes described in the Figs. 5 and 6 from the comparison of geometries. The others are deduced from chemical analyses (Gratier, 1983). Analyses of major element and calcimetry both are used and compared. The results show a good fit between the three techniques for all the layers.

matrix have roughly the same luminescence. These calcite veins may belong to the same generation that probably crystallised from the same fluid.

To further examine the origin of calcite veins, REE measurements have been made with an ICP/MS (Inductively Coupled Plasma Mass Spectrometry),

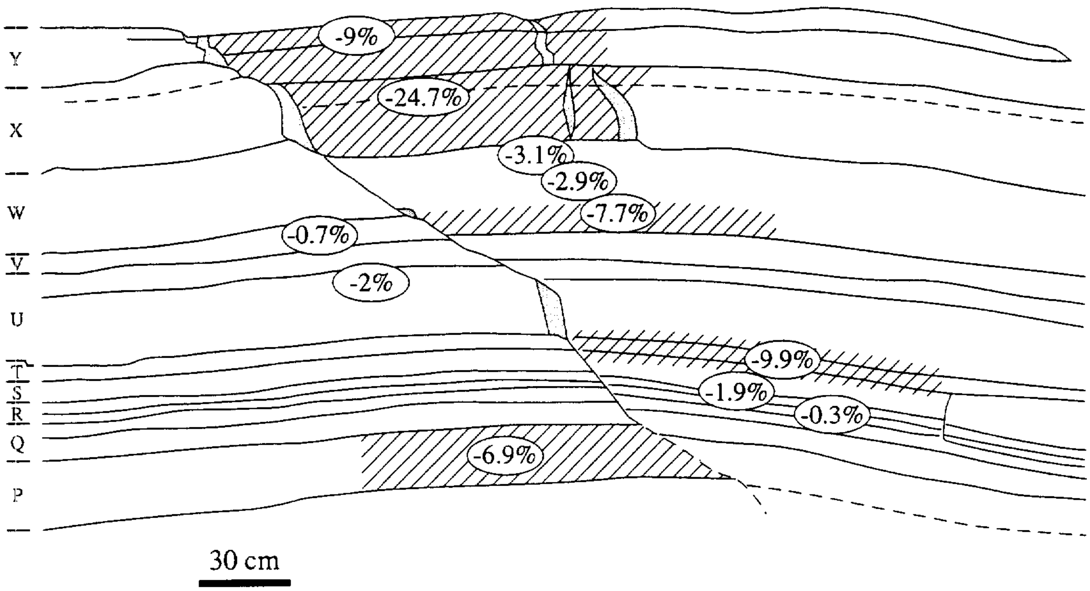

Fig. 11. Measurement of $\Delta V/V$ made from calcimetry around the fault surface. Most of the areas that have lost volume are located in the hanging wall of the fault. Areas of large volume change have been hatched in the figure. The foot wall is relatively protected as shown from the kinematic analyses. The volume loss is most important in the hanging wall but it is not the same for all layers. The volume loss is large (24.7%) in the layer X where $CaCO_3$ content is about 90%. The volume loss is moderate (about 10%) when the $CaCO_3$ content is between 60 and 80% in the layers P, S, U and Y. The volume loss is very low (from 0.7 to 3.1%) when the $CaCO_3$ content is lower than 60%.

on seven samples from five layers (U, P, W, R and X) and a large calcite domino on the fault surface (Fig. 12). All layers, except the calcite domino T_0, have nearly flat patterns compared to the upper crust with concentrations from 0.3 to 0.5 that of the upper crust. This variation is compatible with

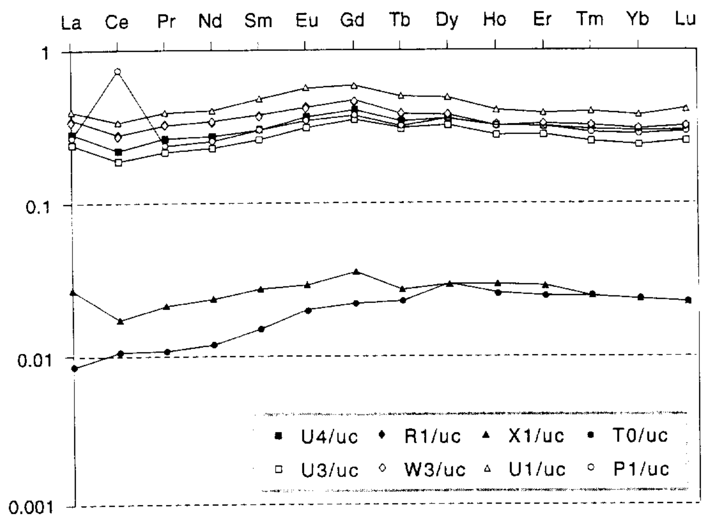

Fig. 12. Plot of rare-earths elements normalized to their average concentrations in the upper continental crust (Taylor and Mc Lennan, 1985). All layers, except for layer X_1 and the calcite domino T_0, have nearly flat patterns and their concentrations vary from 0.3 to 0.5 that of the upper crust. Location of the samples is given Fig. 2.

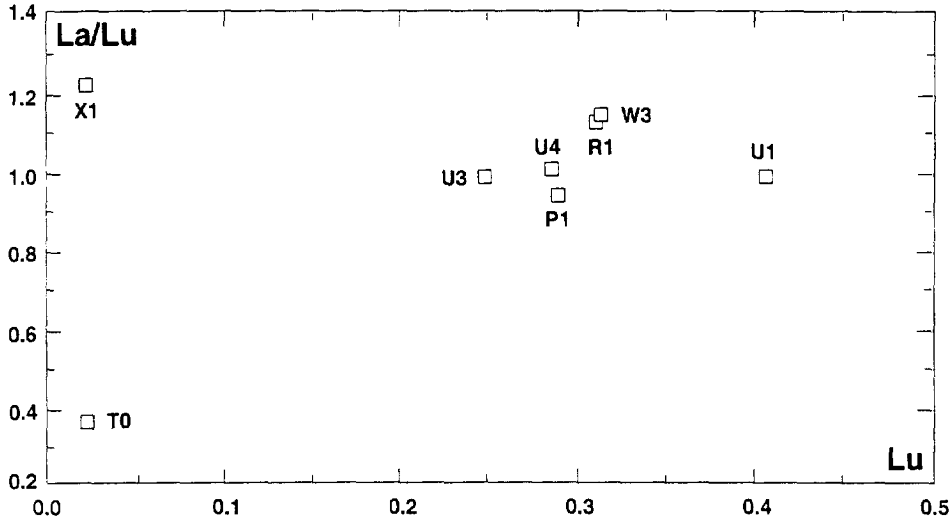

Fig. 13. Plot of normalised La/Lu versus Lu for selected samples showing that all samples, except X_1 and T_0, have almost no fractionation between LREE and HREE.

their flyschoid origin, as all layers are mixtures, with varying proportions, of detrital and carbonaceous components. The detrital component has an identical pattern and concentration, to the upper crust, and the carbonaceous component would act roughly as a diluent. The dilution effect due to the carbonaceous phase is confirmed by sample X_1 which displays a strongly depleted rare-earth element pattern (around 0.02 of the upper crust), in agreement with its $CaCO_3$ content (94%). Sample P_1 displays a cerium (Ce) positive anomaly which can be explained in terms of redox conditions which is beyond our purpose. Calcite domino T_0 alone displays a different pattern with LREE/HREE depletion.

Taking lutetium (Lu) as a representative of the rare-earth element content, a plot of La/Lu, where La is lanthane, versus Lu (Fig. 13) shows that, within layer U, Lu content decreases with decreasing distance to the fault. There is no evident fractionation between light rare-earth elements (LREE) and heavy rare-earth elements (HREE) in layer U while X_1 shows a slight light rare-earth enrichment. Domino T_0 is significantly different from all other samples, being depleted in LREE as compared to HREE, which may be explained by the aqueous geochemistry of the REE's. Wood (1990) showed that carbonate complexing favours LREE over HREE. A carbonate-rich fluid which percolates in this flyschoid formation will extract more easily HREE than LREE, leaving a residue slightly enriched in LREE. This cannot be seen in most of the samples because it is negligible as compared to bulk amount of rare-earth elements, but might be seen in X_1 which has a lower overall content. As a consequence, calcite precipitating from a HREE-enriched fluid will have a rare-earth element pattern enriched in HREE compared to LREE as found in sample T_0. This pattern in calcite is very different from the original flat REE pattern of the carbonaceous phase. Similar patterns in fissural calcite have been described by Bau (1991).

5. Conclusion

– The displacement on the fault surface that constitutes three right-stepping fractures, formed tensile bridges that broke and opened along small left-stepping fractures resulting in the formation of calcite dominos. Displacement on the fault zone is parallel to the fault surface.

– The relative displacement vector field shows that the displacement of the blocks was a non-rigid translation. This means that deformation occurred while displacement was taking place. The deformation was not homogeneous and is concentrated more in the hanging wall.

– Negative volume changes in the hanging wall were balanced by positive volume changes close to the fault surface. This agrees with a displacement parallel to the fault surface.

– Numerous stylolites and calcite veins are obvious evidence for pressure solution that occurred everywhere near the fault. Calcite appears to be the only mineral involved in the pressure solution process.

– Calcite dissolution was most active in the hanging wall. This calcite depletion was not homogeneous in the block but probably favoured in the layers where calcite content was more than 60%.

– Study by cathodoluminescence shows that all the calcite crystals observed in the veins, on the fault surface and in the matrix have roughly the same luminescence, indicating that they formed synchronously from the same fluid

– The rare-earth element contents measured in some layers and in the T_0 domino show that calcite of T_0 came from the immediate vicinity of the fault. LREE depletion in the T_0 domino may reflect the chemistry of the fluid. This fluid leached the flyschoid formation and transported REE as carbonate complexes, the HREE carbonate complexes being stronger than complexes with LREE.

– Our study shows that calcite veins formed during deformation by small-scale mass transfer. No evidence of exogenic calcite coming from outside the formation was found. It is not certain whether any calcite has escaped from the system.

Acknowledgements

We wish to thank the following people for their help with different parts of the study: M. Valladon and B. Reynier during ICP/MS measurements, C. Lucas and D. Béziat with calcimetry measurements, A.M. Roquet, D. Bekadour and M. Thibault with thin sections and cathodoluminescence observations and C. Cavaré-Hester for improving most of the figures. This paper has been significantly improved by the constructive reviews of Stefano Salvi, J.P. Gratier and an anonymous reviewer.

References

Bau, M., 1991. Rare-earth element mobility during hydrothermal and metamorphic fluid–rock interaction and the significance of the oxidation state of europium. Chem. Geol. 93, 219–230.

Bürgman, R., Pollard, D., 1994. Strain accommodated about strike-slip fault discontinuities in granitic rock under brittle-to-ductile conditions. J. Struct. Geol. 16, 1655–1674.

Carrio-Schaffhauser, E., Chenevas-Paule, F., 1989. Quantification géométrique de la dissolution-cristallisation liée à une déformation cassante. Bull. Soc. Géol. Fr. 8, 597–604.

Carrio-Schaffhauser, E., Gaviglio, P., 1990. Pressure solution and cementation stimulated by faulting in limestones. J. Struct. Geol. 12, 987–994.

Chinnery, M.A., 1961. The deformation of the ground around surface faults. Bull. Seismol. Soc. Am. 51, 355–372.

Fletcher, R.C., Pollard, D.D., 1981. Anticrack model for pressure solution surfaces. Geology 9, 419–424.

Frei, L.S., Freund, R., 1990. Spatial and temporal relationships between two sets of strike-slip faults in southeastern Sinai. Tectonophysics 180, 111–122.

Freund, R., 1970. Rotation of strike-slip faults in Sistan, Southeast Iran. J. Geol. 78, 188–200.

Freund, R., 1974. Kinematics of transform and transcurrent faults. Tectonophysics 21, 93–134.

Gamond, J.-F., 1987. Bridge structures as sense of displacement criteria in brittle fault zones. J. Struct. Geol. 9, 609–620.

Gapais, D., Fiquet, G., Cobbold, P.R., 1991. Slip system domains, 3. New insights on fault kinematics from plane-strain sandbox experiments. Tectonophysics 188, 143–157.

Gratier, J.P., 1983. Estimation of volume changes by comparative chemical analyses in heterogeneously deformed rocks (folds with mass transfer). J. Struct. Geol. 5, 329–339.

Gratier, J.P., 1987. Pressure solution–deposition creep and associated tectonic differentiation in sedimentary rocks. In: Jones, M.E., Preston, R.M.F. (Eds.), Deformation of Sediments and Sedimentary Rocks. Geol. Soc. London Spec. Publ. 29, 25–38.

Gratier, J.-P., Gamond, J.-F., 1990. Transition between seismic and aseismic deformation in the upper crust. In: Knipe, R.J., Rutter, E.H. (Eds.). Deformation Mechanisms, Rheology and Tectonics. Geol. Soc. London Spec. Publ. 54, 25–38.

Heald, M.T., 1956. Cementation of Simpson and St. Peter sandstone in part of Oklahoma, Arkansas and Missouri. J. Geol. 64, 16–30.

Mc Coss, A.M., 1986. Simple constructions for deformation in transpression/transtension zones. J. Struct. Geol. 8, 715–718.

Odonne, F., 1990. The control of deformation intensity around a fault: natural and experimental examples. J. Struct. Geol. 12, 911–921.

Odonne, F., Massonnat, G., 1992. Volume loss and deformation around conjugate fractures: comparison between a natural example and analogue experiments. J. Struct. Geol. 14, 963–972.

Peacock, D.C.P., Sanderson, D.J., 1995. Pull-aparts, shear fractures and pressure solution. Tectonophysics 241, 1–13.

Pollard, D.D., Segall, P., 1987. Theoretical displacements and stresses near fractures in rock: with applications to faults, joints, veins, dikes and solution surfaces. In: Atkinson, B.K. (Ed.), Fracture Mechanics of Rocks. Academic Press, London, pp. 277–349.

Ramsay, J.G., 1980. The crack-seal mechanism of rock deformation. Nature 284, 135–139.

Ramsay, J.G., Huber, M.I., 1983. The Techniques of Modern Structural Geology, Volume 1. Strain Analysis. Academic Press, London, 307 pp.

Rispoli, R., 1981. Stress fields about strike-slip faults inferred from stylolites and tension gashes. Tectonophysics 75, T29–T36.

Robert, I., 1979. Etude des mécanismes de plissément d'une série stratifiée dans une zone de cisaillement, exemple de la côte basque. Unpublished thesis, Univ. Grenoble, 244 p.

Schreurs, G., 1994. Experiments on strike-slip faulting and block rotation. Geology 22, 567–570.

Taylor, S.R., Mc Lennan, M., 1985. The Continental Crust: Its Composition and Evolution. Blackwell Scientific Publ., London, 312 pp.

Walsh, J.J., Watterson, J., 1989. Displacement gradients on fault surfaces. J. Struct. Geol. 11, 307–316.

Weyl, P.K., 1959. Pressure solution and force of crystallization, a phenomenological theory. J. Geophys. Res. 64, 2001–2025.

Wood, S.A., 1990. The aqueous geochemistry of the rare earth elements and Yttrium, 1. Review of available low temperature data of inorganic complexes and the inorganic REE speciation of natural waters. Chem. Geol. 82, 159–186.